Topics in Catalysis (2019) 62:56–62
https://doi.org/10.1007/s11244-018-1103-2

ORIGINAL PAPER

Structural Induced Effect of Potassium on the Reactivity of Vanadate Species in V_2O_5–WO_3/TiO_2 SCR-Catalyst

H. Siaka[1] · C. Dujardin[1] · A. Moissette[2] · P. Granger[1]

Published online: 4 December 2018

Abstract
A renewed interest of benchmark $V_2O_5/WO_3/TiO_2$ SCR-catalysts is discernible for the depollution of stationary sources jointly with the use of bio-fuels as substitute to fossil fuels. However, the resistance to deactivation has to be reconsidered according to additional alkaline contamination. This study tried to elucidate the impact of potassium on the stability of vanadate and tungstate species at various dispersions for two different K/V ratios equal to 0.2 and 0.8. Different kinetic behaviors of fresh and K-poisoned catalysts have been discussed based on the affinity of potassium to neutralize preferentially strong acid sites as well as to alter the capability of V=O redox sites.

Keywords Ammonia · V_2O_5–WO_3/TiO_2 · Standard-SCR · Selective Catalytic Reduction · NO_x

1 Introduction

$V_2O_5/WO_3/TiO_2$ catalyst is recognized as a benchmark for end-of-pipe technologies to reduce efficiently NO_x emissions from stationary and mobile sources. Presently, extensive investigations [1–3] led to a relative consensus on the intrinsic catalytic properties of supported mono- and polyvanadate species and detailed insight into the role played by tungsten to create stronger Brønsted acid sites. In addition, these catalytic systems exhibit a relative high tolerance to sulfur and lubricant poisoning [4]. On the other hand, their low thermal stability at high temperature limits their application to stationary sources. Indeed, significant aggregation of well-dispersed vanadate to unselective and volatile V_2O_5 aggregates can occur at high temperature. In addition, significant loss of surface acidity can lead to ammonia slip [5]. As a consequence, fundamental approaches are still of interest in order to clarify the discussions on the reaction mechanisms and to understand the impact of contaminations on the kinetic properties [3].

Today a renewed interest is perceptible related to the substitution of fossil fuels by biofuels containing impurities and inorganic additives that can severely alter the catalytic properties of conventional SCR catalysts through poisoning effects [4]. Potassium and sodium contamination can induce a loss of specific surface area and of density of acid sites. As a consequence an irreversible weakening of ammonia adsorption leads to the deactivation of vanadia-based SCR-catalysts [4]. From a fundamental viewpoint, alkaline incorporation would increase the energy needed for proton abstraction of V–OH groups [6]. On V_2O_5–WO_3/TiO_2 catalysts, the competitive neutralization of W–OH and V–OH can be an important issue to understand deactivation phenomena. Combined DFT and DRIFT spectroscopy studies also revealed that V–OH Brønsted acid sites and V^{5+}=O redox sites can be inhibited [7]. Recent investigation agrees with this conclusion revealing from transient kinetic measurements that alkali contamination preferentially poisons active V^{5+}–OH and/or V^{5+}=O sites instead of titania and tungsten sites [8].

This study is focused on the sensibility of potassium exposure to the reaction rate and selectivity of V_2O_5–WO_3/TiO_2 SCR-catalysts. Particular attention was paid to their behavior at low and high concentration of potassium in order

Electronic supplementary material The online version of this article (https://doi.org/10.1007/s11244-018-1103-2) contains supplementary material, which is available to authorized users.

✉ P. Granger
pascal.granger@univ-lille.fr

[1] Univ. Lille, CNRS, Centrale Lille, ENSCL, Univ. Artois, UMR 8181 -UCCS - Unité de Catalyse et Chimie du Solide, 59000 Lille, France

[2] Univ. Lille, Laboratoire de Spectrochimie Infrarouge et Raman, UMR CNRS 8516, Bâtiment C5, 59650 Villeneuve d'Ascq, France

to check the influence of electronic and structural induced effect on vanadate species as well as the effect of water on these catalysts. Potassium poisoning was obtained by simple wet impregnation insuring a good repeatability [9].

2 Experimental

2.1 Preparation and Physicochemical Characterization

V_2O_5–WO_3/TiO_2 were prepared by successive impregnation of TiO_2-P25 (93 m^2/g) supplied by Degussa. The amounts of precursor salts, *i.e.* ammonium tungsten oxide hydrate and ammonium vanadium oxide, were calculated to obtain on calcined samples surface densities of 9.5 W nm^{-2} and 4 V nm^{-2} respectively. Afterwards, potassium was deposited by wet impregnation with a solution of potassium nitrate in order to get atomic K/V ratio of 0.2 and 0.8. Fresh and K-poisoned samples were calcined in air at 450 °C and labeled W/T, VW/T, VW/T-K2 and VW/T-K8 respectively.

Bulk characterizations were performed by XRD analysis with a Bruker AXS D8 Advance diffractometer. Raman spectroscopic measurements were carried out on a Raman micro-spectrometer Xplora Plus (Horiba Scientific) equipped with Syncerity CCD detector. Raman spectra were recorded by using an excitation wavelength of 638 nm. H_2 temperature-programmed reduction experiments (H_2-TPR) were performed on a Micromeritics Autochem II 2920 analyzer. Samples were exposed to a flow of 5 vol% H_2 in Ar and a temperature gradient of 10°C/min.

XPS measurements were carried out on an AXIS Ultra DLD Kratos spectrometer equipped with a mono-chromatized aluminium source for excitation. All binding energies were referenced to the C 1s core level at 284.8 eV. Specific surface area was measured by N_2 physisorption at − 196 °C with a Flowsorb III analyzer. Ammonia Temperature-Programmed-Desorption experiments were performed on 100 mg catalyst from 120 to 700 °C on a Micromeritics Autochem II 2920 analyzer. The outlet gas mixture was analyzed by an Omnistar Balzers Mass Spectrometer to withdraw the contribution of water and the weak formation of NO_x coming from the oxidation of adsorbed ammonia at high temperature. Prior ammonia adsorption at 120 °C, the samples were degassed in helium at the same temperature. Pre-adsorbed samples were evacuated under He flow to remove physisorbed ammonia.

2.2 Catalytic Measurements

Catalytic measurements were performed in a fixed-bed flow reactor at atmospheric pressure on 200 mg catalyst diluted with 800 mg SiC. The total flow rate was fixed at 15 L h^{-1} for working at constant Gas Hourly Space Velocity of 75,000 mL h^{-1} g^{-1}. The catalytic performances were evaluated from temperature-programmed reaction (TPR) experiments with inlet gas mixture composed of 400 ppm NH_3, 400 ppm NO and 8 vol% O_2 balanced with helium in the presence or in the absence of 10 vol% H_2O. The composition of the outlet gas mixture was monitored by a μGC. Prior to TPR experiments, the samples were treated in air at 450 °C overnight then exposed to the reaction mixture in dry conditions for 3 h. First, the conversions were recorded during the cooling period at constant temperature gradient (TPR1). After stabilization at 160 °C, the conversions were recorded during heating at the same gradient temperature in wet conditions, *i.e* reaction mixture with 10 vol% H_2O (TPR2). Finally, TPR1 conditions were repeated at the end of the sequence to check the effect of water on the catalyst stability (TPR3).

3 Results and Discussion

3.1 Bulk Physicochemical Properties of Fresh and K-Poisoned V_2O_5–WO_3/TiO_2

XRD patterns on calcined samples are compared in Fig. 1. The characteristic reflections of the tetragonal structure of anatase dominate. Additional less intense reflections appear ascribed to the orthorhombic structure of WO_3. The presence of V_2O_5 crystallites was not detected which suggests a good dispersion of vanadate species as reported elsewhere [10]. The absence of bulk detectable potassium species is also noticeable. These structural features can be

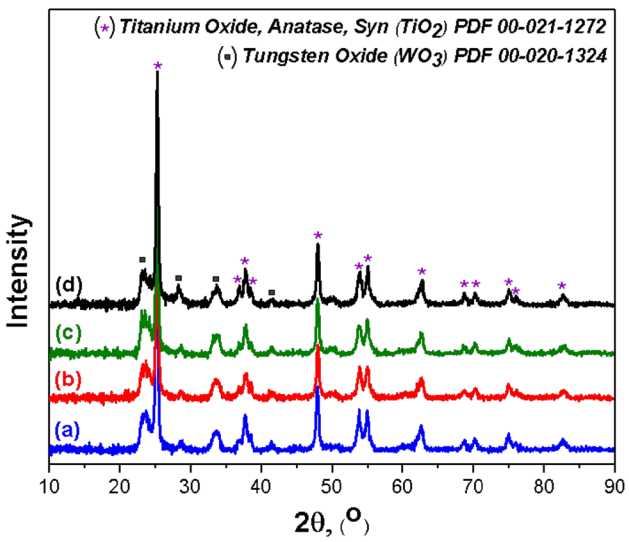

Fig. 1 Powder XRD paterns recorded on W/T (*a*); VW/T (*b*); VW/T-K2 (*c*); WV/T-K8 (*d*) calcined in air at 450°C

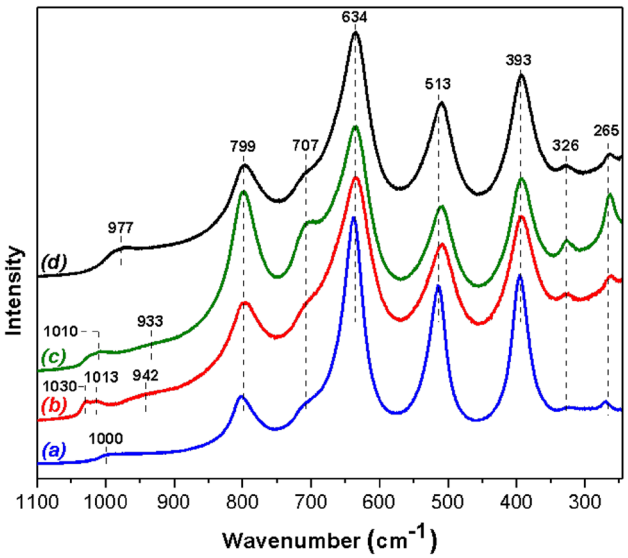

Fig. 2 Raman spectra recorded on W/T (*a*); VW/T (*b*); VW/T-K2 (*c*); VW/T-K8 (*d*) calcined in air at 450°C

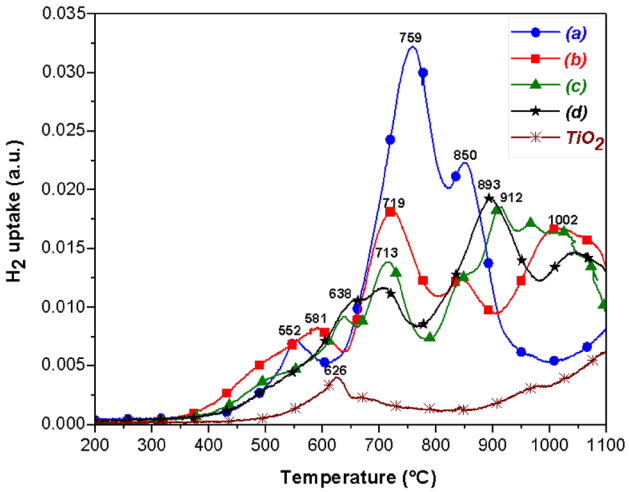

Fig. 3 H_2-Temperature-Programmed-Reduction (H_2-TPR) on calcined W/T (*a*); VW/T (*b*); VW/T-K2 (*c*); VW/T-K8 (*d*)

supplemented by Raman spectroscopy as useful technique to characterize amorphous structures. Anatase can be easily identified through the most intense Raman lines at 799, 634, 513 and 393 cm^{-1} in Fig. 2. The contributions at 707, 265 and 800 cm^{-1} (overlapped by the vibration of anatase) correspond to the W-O stretching mode and W-O-W bending mode of crystalline WO_3 [11]. The weak intensity of V-O-V vibration in the range 933–942 cm^{-1} characterizing polyvanadates and the absence of the 994 cm^{-1} Raman line ascribed to three-dimensional V_2O_5 oxide phase emphasizes the high dispersion of vanadium evidenced by the Raman lines above 1000 cm^{-1} on VW/T generally assigned to terminal V=O bond of isolated vanadate species [12]. As observed, the 1013–1030 cm^{-1} contribution attenuates then disappears at increasing potassium loading progressively replaced by the 977 cm^{-1} Raman line appearing distinctly on VW/T-K8. Similar observations were earlier reported with tentative assignment to K–O–V=O [13] or to tetrahedrally and octahedrally coordinated polymeric tungsten oxide species [14]. Alternatively, a red shift observed on the 1013–1030 cm^{-1} could reflect electronic interaction support $-V{=}O^{\delta-}\ldots K^{\delta+}$, which could induce an elongation of the V=O bond [15].

H_2-TPR profiles reported in Fig. 3 reveal intense and broad signals above 500 °C compared to the bare TiO_2 support which illustrate the reducibility of W(+VI) and V(+V) species. Particular attention was paid to the lowest temperature range, below 800 °C, which could reflect the surface heterogeneity of oxidic vanadium and tungsten species [10]. As seen, three contributions are discernible at 552 °C, 759 °C and 850 °C on W/T. The low temperature reduction process could be related to highly dispersed WO_x species on TiO_2, while a two steps reduction of W(+VI) to W(0) with the intermediate formation W(+IV) would occur for bulk oxidic tungsten species. Significant changes are discernible after vanadium incorporation related to the shift observed on the prominent reduction peak from 759 to 719 °C and a peak widening of the low temperature reduction process characterized by an apparent maximum at 581 °C and a shoulder near 500 °C. Previous investigations reported that well-dispersed VO_x species reduces at relatively low temperature, i.e. 400–500 °C instead of T > 700 °C for bulk species [16, 17] which seems consistent with the segregation of highly dispersed VO_x species on VW/T. Interestingly the low temperature reduction process attenuates on K-poisoned samples shifting to a maximum centered at 687 °C which could be in rather good agreement with a peculiar interaction between VO_x and potassium as suggested from Raman spectroscopy [15]. Let us note that no significant information on the nature of interactions between tungsten and potassium arises from those results despite previous investigations pointed out the important role of oxidic tungsten species acting as sacrificial agent and then preserving the dispersion of vanadia [10].

3.2 Surface Properties of K-Doped and Un-doped V_2O_5–WO_3/TiO_2

3.2.1 Nitrogen Physisorption

Nitrogen physisorption isortherms were recorded at − 196 °C. Adsorption–desorption branches form hysteresis of type IV which characterizes the presence of partially uniform mesopores (not shown). Specific surface area, pore volume and average pore size diameter, calculated by the BET and BJH methods, are listed in Table 1 and compared with the bare anatase support. As seen in Fig. 4 successive

Table 1 Impact of potassium poisoning on the textural properties and reducibility of supported tungstate and vanadate species

Catalyst	S_{BET} (m^2/g)	Pore volume (cm^3/g)	Pore size diameter (nm)	Amount of desorbed NH_3 (μmol/g)	Normalized amount of desorbed NH_3 (μmol/m^2)
TiO_2 (T)	72	0.35	15.2	–	n.m.
W/T	52	0.25	16.8	240	4.6
VW/T	38	0.20	17.8	150	3.9
VW/T-K2	45	0.24	17.5	90	2.0
VW/T-K8	40	0.22	18.6	50	1.2

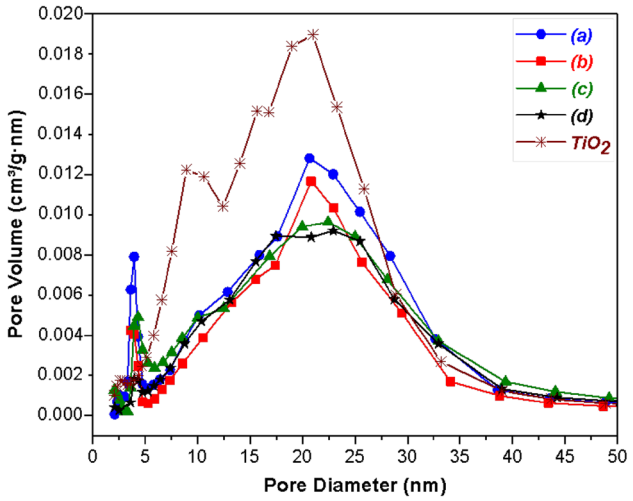

Fig. 4 Pore size distribution from nitrogen physisorption measurements on calcined W/T (*a*); VW/T (*b*); VW/T-K2 (*c*); VW/T-K8 (*d*)

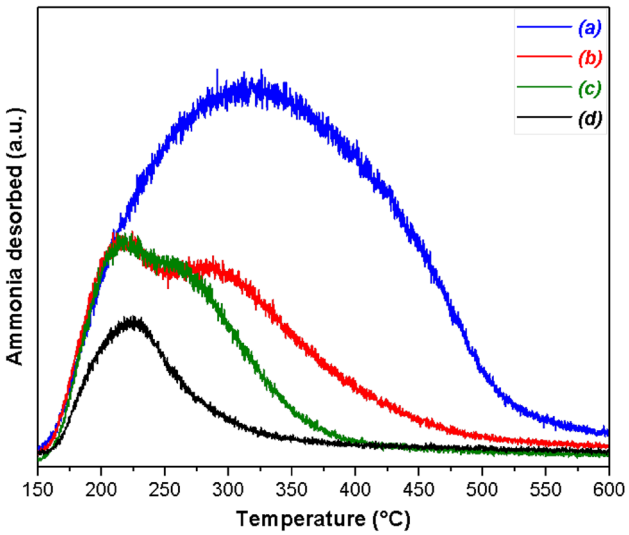

Fig. 5 Ammonia-temperature-programmed-desorption on calcined W/T (*a*); VW/T (*b*); VW/T-K2 (*c*); VW/T-K8 (*d*)

tungsten and vanadium impregnations lead inevitably to a discernible alteration of the porous structure. Interestingly, an additional narrow distribution appears around 5 nm after tungsten deposition which attenuates notably after incorporation of high potassium loading. As a general trend, one can observe that potassium poisoning has a weak sensibility on the textural properties with slight deviations on the specific surface areas and pore volumes compared to WV/T. Such comparison suggests a homogenous potassium deposition through the porous structure of the materials in agreement with the absence of bulk detectable oxidic potassium species from XRD analysis.

3.2.2 Ammonia-Temperature-Programmed Desorption

Broad and intense ammonia TPD curve is observed on W/T in Fig. 5 highlighting the coexistence of weakly and strongly adsorbed NH_3 species on Lewis and Brønsted acid sites [1, 2]. Ammonia desorption on weak acid sites generally takes place below 300 °C [18]. Subsequent incorporation of vanadium to W/T leads to a weaker ammonia desorption (see Fig. 5b; Table 1) likely due to the lower specific surface area of VW/T and a weak oxidation of pre-adsorbed ammonia species with a rise temperature during TPD experiments. Similar features were previously reported on binary V-W samples with a weakening of ammonia adsorption suggesting that strong acid sites on WO_3 would store and facilitate the transport of ammonia to more reactive vanadate active sites [19]. Interestingly, low potassium doping deteriorates the adsorptive properties of VW/T and the strongest adsorption sites seem more affected. At higher potassium loading, i.e. on VW/T-K8, both weak and strong acid sites are deteriorated which seems in relative good agreement with a preferential neutralization of strong acid sites by potassium at low loading possibly ascribed to Brønsted sites as reported elsewhere [6].

3.2.3 Surface XPS Analysis

Particular attention was paid to the analysis of characteristic Ti 2p, V 2p, W 4d, K 2p core levels. The Binding Energy (B.E.) for Ti $2p_{3/2}$ near 459.1 eV characterizes Ti^{4+} stabilized as TiO_2. The photopeak V $2p_{3/2}$ and W $4d_{5/2}$ on fresh

and K-poisoned VW/T samples slightly changes. XPS spectral features are resumed in Table 2 underlining a greater stabilization of W^{6+} [20–22]. Weak and asymetric V $2p_{3/2}$ photopeaks highlight the coexistence of V^{4+} and V^{5+} currently observed in the BE ranges 516.4–516.7 eV and 517.1–517.6 eV respectively. Subsequent decompositions (see Fig. S1 in supplementary information) lead to the estimation of the V^{4+}/V^{5+} ratio in Table 2. Despite the slight decrease observed on the V^{4+}/V^{5+} ratio, this evolution could be an indication of the degree of dispersion of vanadate species. Indeed, Koust et al. [23] found from XPS analysis that V^{4+} ascribed to monomeric VO_2 species are mainly stabilized at sub-monolayer coverage whereas a partial oxidation to V^{5+} is observed for two monolayer coverage. Zhang et al. [24] observed a slight decline of V^{4+}/V^{5+} ratio at increasing vanadium content corresponding to the formation of polymeric vanadate species. Particular attention was also paid to the O 1s photopeak. In practice, the O 1s photopeak can be decomposed in three components as described in Fig. S2 corresponding to lattice oxygen (O^{2-} labeled O_β) near 529.5–530.0 eV, surface chemisorbed oxygen species (O_α) near 531.0–531.6 eV and chemisorbed water ($O_{\alpha'}$) near 532.8–533.0 eV [25]. The values for the ratio O_α/O_T with $O_T = O_\beta + O_\alpha + O_{\alpha'}$ slightly decrease on K-poisoned samples. Despite, no clear potassium dependency of the relative surface concentration of O_α is evidenced such weak effect could reflect the formation of strong chemical bond between potassium and oxygen.

3.3 Catalytic Properties of Fresh and K-Poisoned V_2O_5–WO_3/TiO_2 Comparison with Bulk and Surface Structure

Temperature-programmed NO_x conversion and N_2O selectivity curves in the absence (TPR1 and TPR3) and in the presence of 10 vol% H_2O (TPR2) are reported in Fig. 6. According to the experimental protocol described in "Experimental", TPR3 performed in similar conditions as TPR1 does not reveal significant deviations on the conversion and selectivity that could reflect drastic changes of surface properties during exposure to wet conditions up to 450 °C. It is worthwhile to note that the conversion curves on W/T and VW/T mainly diverge at low temperature in dry conditions which emphasizes the beneficial role played by vanadate species in standard-SCR likely due to the predominance of highly dispersed VO_x species as characterized from Raman spectroscopy. Interestingly, a typical volcano-type curve is restored on K-poisoned VW/T. As seen, SCR conversion decreases significantly above 300 °C becoming lower than that measured on W/T. In this temperature range ammonia oxidation occurs significantly leading to an extra production of NO and a slight production of N_2O. These observations underline the detrimental effect of potassium doping on the selectivity behavior possibly related to a preferential neutralization of strong acid sites ascribed to W–OH or V–OH Brønsted acidity. These observations could reflect in a certain extent the competition to proton abstraction between V–OH and W–OH induced by potassium. A detrimental effect of potassium is also discernible at low temperature. Nevertheless, the residual NO conversion still remains higher than that obtained on W/T. Potassium can also alter the redox capability of vanadium [26] through the formation of strong chemical bond with oxygen coordinated to vanadium. The detrimental effect of potassium on the reducibility of VO_x species is clearly observed from H_2-TPR experiments and could explain the significant loss of rate of NO_x reduction in the whole temperature range. As observed, slight deviation observed on the atomic O_α/O_T ratio agrees with a partial inhibition of oxygen release due to the formation of chemical bond with potassium. A structural explanation given by Due-Hansen et al. [15] from Raman analysis on dehydrated K-doped and un-doped vanadium based catalysts could also match our observations. These authors compared Raman spectral features with DFT calculations which predict that the dimerization of vanadate monomers would be thermodynamically favored in the presence of potassium. Such an explanation seems in relative good agreement with the slight evolution observed on the V^{4+}/V^{5+} ratio suggesting a slight aggregation induced by potassium. Hence, polymerization of monomeric at increasing potassium content could also reasonably explain the loss of selectivity observed at high temperature in connection with the appearance of the 977 cm^{-1} Raman line on WV/T-K8 ascribed to support $-V{=}O^{\delta-}\cdots K^{\delta+}$ interaction.

Table 2 XPS analysis of K-doped and undoped V_2O_5–WO_3/TiO_2

Catalyst	B.E. (eV)[a]				Surf. composition[a]					
	Ti $2p_{3/2}$	V $2p_{3/2}$	W $3d_{5/2}$	K $2p_{3/2}$	V/Ti	V^{4+}/V^{5+}	W/Ti	V/W	K/W + V	O_α/O_T
W/Ti	459.1	–	247.6	–	–		0.14	–	–	0.24
VW/Ti	459.2	516.4/517.5	247.7	–	0.12	0.63	0.14	0.90	–	0.23
VW/T-K2	459.0	516.2/517.3	247.3	292.9	0.13	0.60	0.14	0.90	0.11	0.18
VW/T-K8	459.0	516.2/517.3	247.4	292.9	0.12	0.52	0.15	0.80	0.27	0.19

[a]Binding energy values and surface composition from XPS analysis: accuracy on B.E. values ± 0.2 eV

$O_T = O_\beta + O_\alpha + O_{\alpha'}$

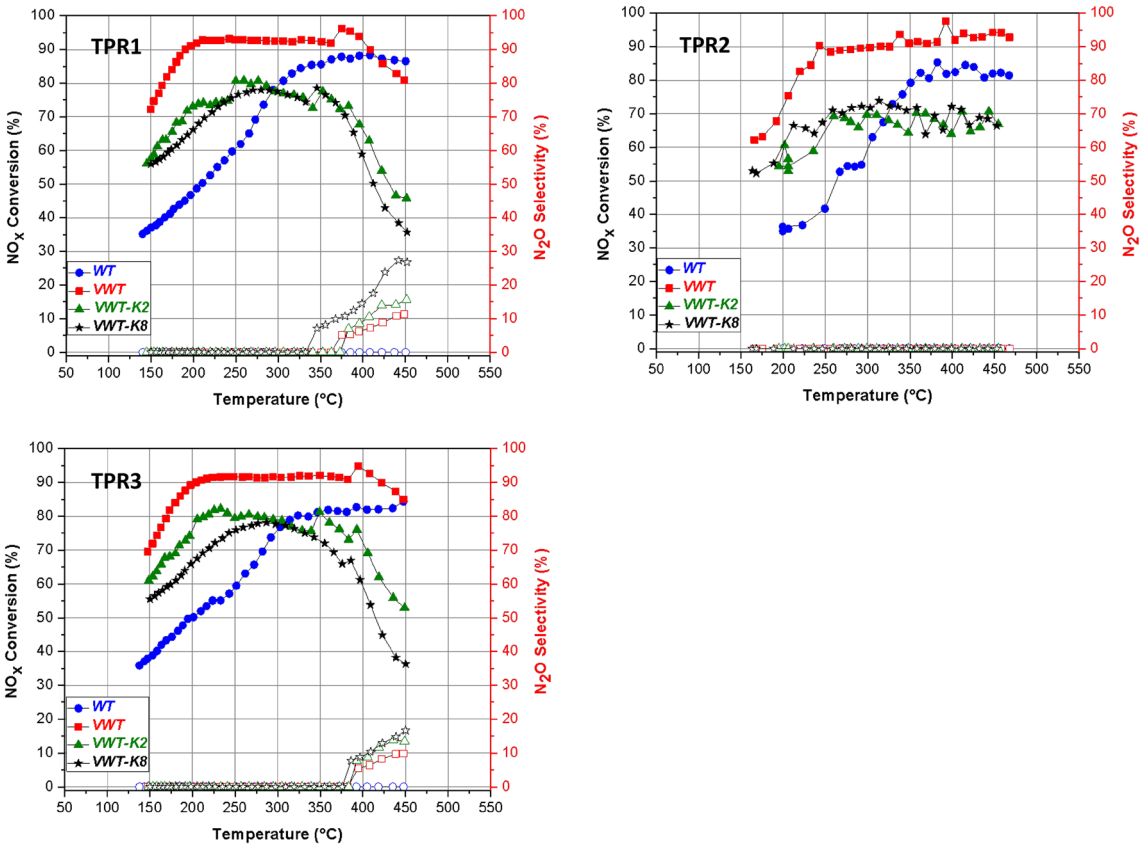

Fig. 6 Ammonia-SCR temperature-programmed experiments on calcined fresh and K-poisoned V_2O_5–WO_3/TiO_2 catalysts: full symbol (NO_x conversion); empty symbol (N_2O selectivity)—W/T (circle); VW/T (square); VW/T-K2 (triangle); VW/T-K8 (star). Reaction conditions: 400 ppm NO, 400 ppm NH_3, 8 vol% O_2 in the absence of water (TPR1, TPR3) and in the presence of 10 vol% H_2O (TPR2) balanced with He, GHSV = 75.000 mL h^{-1} g^{-1}

Significant changes in conversion occur at high temperature in wet conditions, i.e. in the presence of 10 vol% H_2O. As seen, TPR2 highlights a strong rate enhancement in NO_x reduction on VW/T with a high NO_x conversion observed in the range 350–500 °C. Such observation cannot be easily explained and could be related to the interplay between NH_3 or NH_4^+ intermediates bonded to Lewis and Brønsted acid sites respectively [27]. The creation of additional Brønsted acid sites through the hydrolysis of molecular vanadate and tungstate Lewis centers could partly explain the changes observed on the selectivity more in favor of ammonia-SCR. Even though the evolution is much less accentuated such an explanation seems to be still valid to describe the behavior of K-poisoned samples.

Supplementary steady-state kinetic measurements performed at 160 °C confirm this behavior with an apparent reaction order with respect to water concentration almost nil on un-doped and K-poisoned samples (results not shown). This observation underlines the absence of significant inhibiting effect of water ascribed to the displacement of weakly adsorbed ammonia species by water in rather good agreement with the interconversion on Lewis to Brønsted acid sites when water is added to the reaction mixture.

4 Conclusion

The poisoning effect of potassium was investigated on $V_2O_5/WO_3/TiO_2$ SCR-catalysts revealing a strong deactivation in the whole range of temperature compare to parent catalyst. Surface characterization did not reveal a significant loss of specific surface area. XPS analysis only shows weak changes on the spectral features of V and W species but they could be significant. The trend observed on the O_α/O_T emphasizes a deterioration of the reducibility of VO_x centers ascribed to potassium addition which inhibits the release of oxygen. In addition the weak evolution observed on V^{4+}/V^{5+} could reflect the detrimental effect of potassium in the stabilization of well-dispersed VO_x species. More prominent observations are observed on the acidic properties with a sharp decrease of the number of acid sites after K poisoning. A preferential neutralization of strong acid sites would occur leading to a

more pronounced ammonia oxidation at high temperature. Tungsten could act as sacrificial agent preserving vanadate species to deactivation through neutralization.

Water addition to the reaction mixture clearly improves the catalytic performance of VW/T ascribed to the hydrolysis of less selective Lewis acid center. This is confirmed from steady state rate measurements highlighting the water dependency of the rate underlining the predominant stabilization of Brønsted acid sites.

Acknowledgements The authors would like to thank the Region Hauts de France and ADEME for supporting this work through a Ph'D grant (H. Siaka). We greatly acknowledge Dr. Pardis Simon and Olivier Gardoll who conducted XPS measurements and thermal analysis.

References

1. Busca G, Lietti L, Ramis G, Berti F (1998) Appl Catal B 18:1–36
2. Forzatti P (2001) Appl Catal A 222:221–236
3. Lai JK, Wachs IE (2018) ACS Catal 8:6537–6551
4. Guan B, Zhan R, Lin H, Huang Z (2014) Appl Therm Eng 66:395–414
5. Marberger M, Elsener M, Ferri D, Kröcher O (2015) Catalysts 5:1704–1720
6. Chen JP, Yang RT (1990) J Catal 125:411–420
7. Nicosia D, Czekaj I, Kröcher O (2008) Appl Catal B 77:228–236
8. Xie X, Lu J, Hums E, Huang Q, Lu Z (2015) Energy Fuels 29:3890–3896
9. Dahlin S, Nilsson M, Bäckström D, Bergman SL, Bengtsson E, Bernasek SL, Pettersson LJ (2016) Appl Catal B 183:377–385
10. Kompio PGWA, Brückner A, Hipler F, Auer G, Löffler E, Grünert W (2012) J Catal 286:237–247
11. Mamede AS, Payen E, Grange P, Poncelet G, Ion A, Alifanti M, Parvulescu VI (2004) J Catal 223:1–12
12. Bañares MA, Wachs IE (2002) J Raman Spectrosc 33:359–380
13. Chen C, Wu X, Yu W, Gao Y, Weng D, Shi L, Geng C (2015) Chin J Catal 36:1287–1294
14. Kobayashi M, Miyoshi K (2007) Appl Catal B 72:253–261
15. Due-Hansen J, Boghosian S, Kustov A, Fristrup P, Tsilomelekis G, Ståhl K, Christensen CH, Fehrmann R (2007) J Catal 251:459–473
16. Koranne MM, Goodwin JG, Marcelin G (1994) J Catal 148:369–377
17. Youn S, Jeong S, Kim DH (2014) Catal Today 232:185–191
18. Putluru SSR, Riisacher A, Fehrmann R (2010) Appl Catal B 97:333–339
19. Kleemann M, Elsener M, Koebel M, Wokaun A (2000) Appl Catal B 27:231–242
20. Varga M, Lopez DM, Murphy NR, Grant JT, Ramana CV (2015) Appl Surf Sci 353:728–734
21. Demeter M, Neumann M, Reichelt W (2000) Surf Sci 454–456:41–44
22. Dong GJ, Zhao Y, Zhang YF (2014) J Fuel Chem Technol 42(9):1093–1101
23. Koust S, Reinecke BN, Adamsen KC, Beinik I, Handrup K, Li Z, Moses PG, Schnadt J, Lauritsen JV, Wendt S (2018) J Catal 360:118–126
24. Zhang S, Liu S, Hu W, Zhu X, Qu R, Wu W, Zheng C, Gao X (2019) Appl Surf Sci 466:99–109
25. Kwon DW, Park KH, Hong SC (2016) Chem Eng J 284:315–324
26. Kong M, Liu Q, Zhou J, Jiang L, Tian Y, Yang J, Ren S, Li J (2018) Chem Eng J 348:637–643
27. Rasmussen SB, Portela R, Bazin P, Ávila P, Bañares MA, Daturi M (2018) Appl Catal B 224:109–115